Water Science & Technology

Water Science & Technology Vol 89 No 11, 2991 doi: 10.2166/wst.2024.170

Functional and financial analysis of an inclined step solar desalination using phase change nanomaterials

Ahmed Mahal[a,*], Maysoon Al-Haideri[b], Anas Alkhouri[c], Ahmad J. Obaidullah[d] and Meitao Duan[e]

[a] Department of Medical Biochemical Analysis, College of Health Technology, Cihan University-Erbil, Erbil, Kurdistan Region, Iraq
[b] Pharmacy Department, School of Medicine, University of Kurdistan Hewlêr, Erbil, Kurdistan Region, Iraq
[c] College of Pharmacy, Cihan University-Erbil, Erbil, Kurdistan Region, Iraq
[d] Department of Pharmaceutical Chemistry, College of Pharmacy, King Saud University, Riyadh, Saudi Arabia
[e] School of Pharmacy, Xiamen Medical College, Xiamen, China
*Corresponding author. E-mail: ahmed.mahal@cihanuniversity.edu.iq

ABSTRACT

Recent decades have seen a shortage of water, which has led scientists to concentrate on solar desalination technologies. The present study examines the solar water desalination system with inclined steps, while considering various phase change materials (PCMs). The findings suggest that the incorporation of PCM generally enhances the productivity of the solar desalination system. Additionally, the combination of nanoparticles has been used to PCM, which is a popular technique utilized nowadays to improve the efficiency of these systems. The current investigation involves the transient modeling of a solar water desalination system, utilizing energy conservation equations. The equations were solved using the Runge–Kutta technique of the ODE23s order. The temperatures of the salt water, the absorbent plate of the glass cover, and the PCM were calculated at each time. Without a phase changer, the rate at which fresh water is produced is around 5.15 kg/m^2·h. The corresponding mass flow rates of paraffin, *n*-PCM I, *n*-PCM III, *n*-PCM II, and stearic acid are 22.9, 28.9, 5.9, 11.9, and 73 kg/m^2·h. PCMs, with the exception of stearic acid, exhibit similar energy efficiency up to an ambient temperature of around 29°. However, at temperatures over 29°, *n*-PCM II outperforms other PCM.

Key words: economic analysis, energy conservation equations, phase change materials, Runge–Kutta technique, solar desalination technologies

HIGHLIGHTS

- The present study examines the solar water desalination system with inclined steps, while considering various phase change materials (PCMs).
- The findings suggest that the incorporation of PCM generally enhances the productivity of the solar desalination system.

1. INTRODUCTION

Water is an essential resource for all life on Earth. It makes up about two-thirds of the human body, with the blood, lungs, and brain containing 95, 90, and 82% water, respectively (Srinivas *et al.* 2016; Alhamami *et al.* 2024). Even a 2% deficiency in bodily water can lead to detrimental effects (Srinivas *et al.* 2016). The usage of water varies greatly between developed and developing nations. In less developed countries, 89% of water is used for agriculture, 9% for industry, and just 2% for domestic purposes (Tsani *et al.* 2020). Conversely, in industrialized nations, the proportions are 30% for agriculture, 59% for industry (Zamani *et al.* 2023a), and 11% for residential use (Rezaei Rad *et al.* 2023). The scarcity of clean, potable water has emerged as a critical challenge to human sustainability in recent times (Mishra 2023).

The maximum allowable salt concentration in drinking water is 1,000 milligrams per liter. In the industrial sector, the presence of high levels of salts in hard water not only poses a risk of corrosion but also leads to significant issues in the facilities (Zamani *et al.* 2023b). This includes the formation of deposits in pipes and devices, resulting in substantial financial losses (Loreti Hupsel *et al.* 2024). To address this issue, it is imperative for human society to establish methods for supplying potable water (Mishra *et al.* 2021; Zhang *et al.* 2023). Given the exorbitant expenses and ecological challenges associated with fossil

fuels, the utilization of solar energy in nations like Iraq, specifically for the purpose of solar distillation of saline seawater or unpleasant subterranean water sources, presents a viable means of generating potable water (Yang *et al.* 2023).

Extensive research has been conducted on solar water desalination technologies (Bekheet *et al.* 2023). In general, desalination technologies can be divided into three main categories: thermal, membrane, and crystallization. Several technologies, such as reverse osmosis, ion electrodialysis, and steam condensation, are employed to purify water and remove impurities (Amani & Kolliopoulos 2023; Loreti Hupsel *et al.* 2024). However, these methods are costly and exhibit a limited capacity for producing fresh water. Sun water desalination plants employ sun energy to desalinate water, distinguishing them from traditional desalination technologies (Aghajani Afghan *et al.* 2023; Majumder *et al.* 2023). This approach is environmentally sustainable (Bressmann 2004). Kalogirou (2005) possessed a comprehensive understanding of desalination systems and categorized solar desalination into two distinct groups: active and passive (Boukhriss *et al.* 2023). Kabeel (2009) investigated a solar desalination structure with a pyramidal cover of glass and a domed absorber plate. The findings indicate that the mean freshwater output is 4.1 L per square meter, while the system's maximum efficiency is approximately 45%. Additionally, the price of every liter of pure water was approximated to be $0.065. By opting for the thermal photovoltaic solar collector, it is possible to generate the necessary electrical power to pump salt water in forced displacement mode within the desalination system. During the night, the absence of sunshine renders this particular desalination plant incapable of generating fresh water. By including a phase change material (PCM) into the desalination system, it becomes feasible to generate potable water during nighttime hours (Dhivagar *et al.* 2021). Throughout the day, the PCM has the capacity to retain excess heat generated during desalination. During the night, it releases the stored heat, leading to the evaporation of salt water and the ongoing generation of fresh water inside the system. Shanmugan *et al.* (2024) focused on the integration of solar PV technology with stationary solar desalination units as the most sustainable solution in their study. In these integrated systems, the electrical energy generated by solar PV is strategically used to heat the inlet preheaters, increase the air temperature, and optimize the evaporation and condensation processes in the solar desalination unit, consequently enhancing its overall performance (Shanmugan *et al.* 2024).

Tamini (1987) did an experiment that investigated the influence of integrating interior reflectors on the efficiency of solar water desalination. They also conducted experiments to evaluate the performance of water desalination with a single coating with internal reflective mirrors for system side walls. The results indicated an improvement in system efficiency and effectiveness. Using reflectors was advantageous. Several further sources (Khalifa & Ibrahim 2009; Tanaka 2009a, 2009b) have extensively examined the use of reflectors in desalination. A separate team of researchers conducted a study with the aim of enhancing the condensation process in the system through the utilization of both internal and external condensers. Tiwari *et al.* (1997) examined a desalination system that utilized two condensing chambers. In this steam model, a portion of the steam is distilled within the first chamber, while another portion is directed to the second chamber for distillation. The findings of their research demonstrated that this alteration resulted in a rise in the rate of freshwater production.

Multiple studies (Fath & Hosny 2002; Al-Kharabsheh & Yogi 2003; El-Samadony *et al.* 2015) have explored the utilization of condensers in conjunction with desalination systems to enhance the condensation process and augment output capacity. Kabeel & Abdelgaied (2016) examined the impact of incorporating a phase change agent in a desalination system including an inclined surface, under the climatic conditions of Egypt. Their findings demonstrated that the daily output of fresh water in the presence of the phase changer is approximately 67.18% greater than the typical rate. The findings indicate that the thickness of these materials has negligible impact on the desalination output, and A48 was identified as the most optimal PCM. Rabhi *et al.* (2017) employed an absorber plate equipped with fins and an external condenser to enhance the efficiency of a solar desalination plant operating with a single pond. The findings demonstrated a significant 42% enhancement in the desalination output when utilizing fins and condenser in comparison to the single basin desalination system without fins and condenser. Hansen & Murugavel (2017) integrated it with a basic single-pond sun desalination system and a hot water storage tank to enhance the efficiency of the inclined solar desalination plant. In addition, they utilized three variations of grooved and fin-shaped flat plates as the inclined absorber plates for desalination purposes. The findings indicated that the most effective design for an absorbent plate is in the shape of fins. Furthermore, the combined system utilizing this type of absorbent plate demonstrated an efficiency of 46.9%.

Kabeel *et al.* (2018) employed sand as a medium for storing energy and utilized hemp cloth as a wick to enhance the effectiveness of a solar desalination plant operating with a single pond. The findings indicated that the quantity of output generated and the effectiveness of the upgraded desalination facility exhibited improvement in comparison to the basic single-pond desalination plant. A new stepped desalination facility by Saadi *et al.* (2018) increased the productivity of a single-pond solar desalination plant. The utilization of a multi-tray internal vaporizer resulted in an enhanced amount of vaporization. Their findings demonstrated a 47% augmentation in crop production across various seasons throughout the year. In another study, Asbik *et al.*

(2016) studied solar desalination facility exergy that utilized a PCM in the specific climate of Errachidia, Morocco. The researchers also explored the primary factors that influenced the decline in exergy inside the system. Sharon *et al.* (2017) conducted a study on a gradient solar desalination system, examining its environmental and economic aspects in relation to the use of porous materials. Their findings indicated that the slanted solar desalination plant has an annual freshwater production rate that is 19.76% greater than the traditional method. The investment has a payback period of 2.8 years, and over a span of 20 years, the system would effectively mitigate the release of 17.65 tons of carbon dioxide into the environment. Fayaz *et al.* (2024) demonstrated in their study that adding nanoparticles to PCMs is a novel approach to enhancing their thermal energy storage capacity and thermal conductivity. Inspired by this finding, their numerical study investigates the impact of incorporating silicon carbide nanoparticles into paraffin wax as a thermal energy storage material in a semi-cylindrical solar water desalination system. The results clearly indicate that the phase transition from solid to liquid PCM is significantly influenced by the addition of nanoparticles, leading to an increased heat transfer rate. During the initial 60 min, the melting fraction and temperature of the PCM remain uniform. However, as the time exceeds 60 min, the behavior of the PCM changes abruptly, which clearly demonstrates the random distribution of nanoparticles within the PCM. Ibrahim *et al.* (2017) examined the economic exergy and optimization of a solar desalination facility that utilizes an external condenser. The findings of their research indicated that under ideal conditions, the expenditure on exergy degradation and economic exergy will fall by 36 and 45%, respectively.

In 2017, Rahbar *et al.* (2017) performed an empirical investigation on the exergy efficiency and economic evaluation of a two inclined solar desalination facility that was fitted with a thermoelectric heating module. The researchers determined that the exergy efficiency consistently rises over the course of the experiment, with the system reaching a maximum exergy efficiency of approximately 25%. The highest level of efficiency is found at 3:00 p.m., and generally, the efficiency of exergy and the surrounding temperature have an opposite connection. In addition, from an economic perspective, it has been determined that the daytime production cost of water is 0.1422 $/L, whereas the nighttime production cost is 0.237 $/L. This suggests that the nocturnal water production cost is approximately 160% greater than the diurnal cost. In 2017, a study conducted by Yazdanpanahi & Sarhaddi (2017) examined the rate of irreversibility in a thermal photovoltaic collector. The researchers found that optimizing the mass flow rate at 0.002 kg/s reduces the system's irreversibility. The system's irreversibility is most affected by the collector-sun temperature difference's irreversibility number, 66. The loss of heat and water flow friction irreversibility numbers can be ignored. In 2018, Al-harahsheh *et al.* (2018) performed a laboratory test to evaluate pond solar desalination plant efficiency that was linked to a traditional solar collector. Additionally, to accumulate energy, they employed a sequence of cylinder blocks housing PCMs within the desalination pond. The system investigated by them has the capacity to generate approximately 4, 300 day ml/m^2 of fresh water during the day, accounting for approximately 40% of the fresh water produced at night as a result of utilizing PCM.

In the current study, the inclined step desalination system is investigated in the presence of different PCM and thermal collector. Utilizing various PCMs concurrently to analyze the thermodynamics of the inclined step solar desalination system, equipped with a thermal collector, represents a novel approach that has not been previously explored in existing research and analyses. Also, the combination of nanoparticles has been used in PCM, which is one of the common methods to increase the performance of these systems today. The thermal collector enhances the generation of potable water by preheating salt water during daylight hours, while the phase changer enables the creation of fresh water even during nighttime. All the components of the system are considered as control volume and their governing equations are solved in MATLAB software. The thermo-economic analysis of the combined system has been conducted in this research.

2. METHODOLOGY

This section presents an in-depth analysis of the energy dynamics within the solar water desalination system equipped with a PCM and a thermal collector. The primary objective here is the development of a mathematical model for calculating the temperatures of various critical components within the system. These components include the glass cover, the absorber plate, the PCM itself, and the saline water residing in the desalination pond.

- Deriving the governing equations:

An energy balance approach is employed to achieve this objective. By applying this principle to each individual component of the system, a set of non-linear ordinary differential equations is formulated. These equations represent the transient behavior of the system, signifying how temperatures change over time. The specific energy conservation equations are developed for each component, including the PCM, glass cover, absorber plate, and the saline water.

- Solving the model: A computational approach

The governing equations obtained are non-linear. To solve them and determine the desired temperature values, a numerical method known as the fourth-order Runge–Kutta method is utilized. This method provides an efficient and accurate way to solve differential equations.

- Leveraging software for efficiency:

The computational aspect of the model is implemented using MATLAB software. Within MATLAB, the built-in function ODE23s is employed to solve the system of equations. This function utilizes the fourth-order Runge–Kutta method internally.

- Extracting meaningful results:

By solving the model with ODE23s, the temperatures of the saline water (T_w), absorbent plate (T_p), glass cover (T_g), and PCM (T_{PCM}) are obtained at each timestep. This data provides valuable insights into the thermal behavior of the system.

- Validating the model:

To ensure the accuracy of the model, a comparison is made between the predicted temperatures and experimental data obtained from the research of Sarhaddi *et al.* (2017). The root-mean-square error (RMSE) is then calculated for each component. A low RMSE value indicates good agreement between the model's predictions and the experimental data, strengthening confidence in the model's validity.

Finally, an investigation is conducted into the influence of various functional and design parameters on the system's energy efficiency. This analysis helps to identify optimal design configurations that maximize the system's performance. By employing a comprehensive mathematical model and leveraging computational tools, this section provides a deep understanding of the energetic behavior of the solar desalination system. This knowledge is crucial for optimizing the system's design and operation, ultimately leading to a more efficient and productive desalination process.

2.1. Research hypothesis

This section outlines the key hypothesis employed in the mathematical modeling of the solar water desalination system. These hypotheses simplify the model while ensuring its accuracy in predicting the system's behavior.

- Uniform PCM temperature: Due to the thinness of the PCM, we assume a uniform temperature distribution throughout its length at any given time. This simplifies the calculations as we do not need to account for temperature variations within the PCM.
- Stagnant water layer: The model incorporates a layer of stagnant water with a consistent thickness. This stagnant layer represents the water that remains relatively motionless within the desalination system. By assuming a constant thickness, we can avoid complex calculations involving fluid dynamics within this layer.
- Negligible lateral heat transfer: Heat exchange between the sides of the system is considered insignificant. This assumption is valid for well-insulated systems where heat loss through the sides is minimal compared to the heat transfer processes within the core components.
- No steam leakage: The model assumes a closed system with no escape of steam. This simplifies the analysis by eliminating the need to account for vapor losses, which can be minimal in well-sealed desalination units.

These simplifying hypotheses allow us to develop a tractable and efficient mathematical model for the solar water desalination system. The validity of these hypotheses will be further evaluated by comparing the model's predictions with experimental data.

2.2. Energy balance equation for glass coating

Figure 1 illustrates the energy input and output fluxes to the glass cover in a schematic manner.

By formulating the energy equilibrium equation for the glass coating during the transitional phase, we may derive (Sarhaddi *et al.* 2017).

$$\alpha_g I(t) A_g + h_2 A_w (T_w - T_g) = h_{c,g-a} A_g (T_g - T_a) + h_{r,g-s} A_g (T_g - T_s) + (m_g C_g)\left(\frac{dT_g}{dt}\right) \quad (1)$$

$$h_2 = h_{rw} + h_{cw} + h_{ew} \quad (2)$$

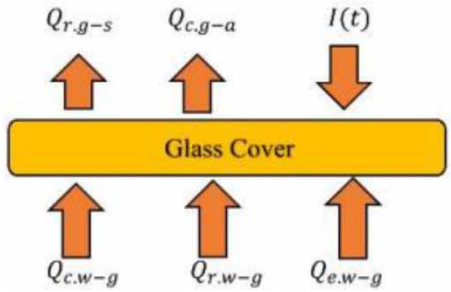

Figure 1 | Northern scheme of energy balance for glass cover.

The coefficient of heat transfer from the surface of the water to the cover of glass is represented as h_2. One crucial parameter in the modeling of solar water desalination plants is the heat transfer coefficient from the water's surface to the glass cover. Please take note that Kumar and Tiwari's equation (Tiwari & Sahota 2017) was utilized (Sarhaddi *et al.* 2017) because of the shortcomings in Dunkel's equation. Using the Tiwari model and experimental data on solar water desalination without a phase changer in Baghdad weather conditions, the displacement heat transfer coefficient was determined. The Appendix section presents the correlation between the modified Prontel number (Pr) and Grashof number (Gr), using the calculated coefficients and convective heat transfer coefficient (Sarhaddi *et al.* 2017).

2.3. Energy balance equation for salt water

According to Figure 2, the amount of energy that the salt water absorbs from the sun and the absorbent plate is the same as the total amount of heat lost through convective heat transfer, evaporative heat transfer, and radiation heat transfer between the water and the glass cover. This can be expressed as follows (Sarhaddi *et al.* 2017):

$$Ir_{\mathrm{w}} = Ex_{\mathrm{des,w}} = \alpha_{\mathrm{w}}\tau_{\mathrm{g}}Ex_{\mathrm{sun}} + Ex_{\mathrm{p-w}} - Ex_{\mathrm{ew}} - \frac{dEx_{\mathrm{w}}}{dt} \tag{3}$$

The exergy rate applied by the absorbent surface to the saline water is calculated using this formula:

$$Ex_{\mathrm{p-w}} = h_1 A_{\mathrm{p}}(T_{\mathrm{p}} - T_{\mathrm{w}})\left(1 - \frac{T_{\mathrm{a}} + 273}{T_{\mathrm{p}} + 273}\right) \tag{4}$$

2.4. Energy balance equation for absorber plate3

Figure 3 illustrates the energy input and output streams directed toward the absorber plate.

$$\alpha_{\mathrm{p}}\tau_{\mathrm{g}}\tau_{\mathrm{w}}I(t)A_{\mathrm{p}} = h_1 A_{\mathrm{p}}(T_{\mathrm{p}} - T_{\mathrm{w}}) + A_{\mathrm{p}}\left(\frac{k_{\mathrm{PCM}}}{x_{\mathrm{PCM}}}\right)(T_{\mathrm{p}} - T_{\mathrm{PCM}}) + (m_{\mathrm{p}}C_{\mathrm{p}})\left(\frac{dT_{\mathrm{p}}}{dt}\right) \tag{5}$$

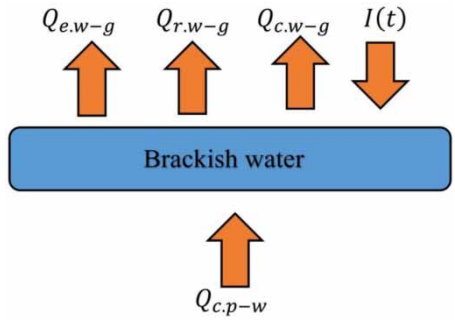

Figure 2 | Schematic of energy balance for salt water.

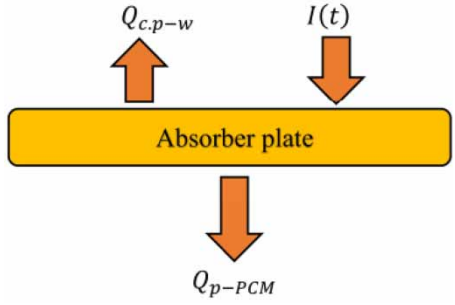

Figure 3 | Schematic diagram of the energy balance for the absorber plate.

k_{PCM} represents the thermal conductivity coefficient of the PCM, whereas x_{PCM} represents its thickness.

2.5. Energy balance equation for PCM

This material is positioned beneath the absorber plate, where it absorbs the energy received from the absorber plate and releases a minimal quantity of it to the surrounding environment. In order to reduce heat loss, a layer of insulation is positioned beneath the PCM (Figure 4). This insulation layer has a particular width and thermal conductivity coefficient. The governing energy equation for the PCM is represented by the following equations (Sarhaddi *et al.* 2017):

$$Ir_{\mathrm{PCM}} = Ex_{\mathrm{des,PCM}} + Ex_{\mathrm{ins-a}} = Ex_{\mathrm{p-ins}} - \frac{dEx_{\mathrm{PCM}}}{dt} \tag{6}$$

$$Ex_{\mathrm{ins-a}} = \left(\frac{k_{\mathrm{ins}}}{x_{\mathrm{ins}}}\right) A_p (T_{\mathrm{PCM}} - T_{\mathrm{a}}) \left(1 - \frac{T_{\mathrm{a}} + 273.15}{T_{\mathrm{PCM}} + 273.15}\right) \tag{7}$$

$$\left(\frac{k_{\mathrm{PCM}}}{x_{\mathrm{PCM}}}\right)(T_{\mathrm{p}} - T_{\mathrm{PCM}}) = \left(\frac{k_{\mathrm{ins}}}{x_{\mathrm{ins}}}\right)(T_{\mathrm{PCM}} - T_{\mathrm{a}}) + \left(\frac{M_{\mathrm{equ}}}{A_{\mathrm{p}}}\right)\left(\frac{dT_{\mathrm{PCM}}}{dt}\right) \tag{8}$$

x_{ins} and k_{ins} are the measure of the thickness and thermal conductivity of the insulating material, respectively.

The PCM's equivalent heat capacity (M_{equ}) is partitioned according to the phases it undergoes during system operation, as described in reference (Sarhaddi *et al.* 2017).

$$\begin{aligned} M_{\mathrm{equ}} &= m_{\mathrm{PCM}} C_{\mathrm{s,PCM}} \quad \text{for } T_{\mathrm{PCM}} < T_{\mathrm{m}} \\ M_{\mathrm{equ}} &= m_{\mathrm{PCM}} L_{\mathrm{PCM}} \quad \text{for } T_{\mathrm{m}} \leqslant T_{\mathrm{PCM}} \leqslant T_{\mathrm{m}} + \delta' \\ M_{\mathrm{equ}} &= m_{\mathrm{PCM}} C_{\mathrm{1,PCM}} \quad \text{for } T_{\mathrm{PCM}} > T_{\mathrm{m}} + \delta' \end{aligned} \tag{9}$$

L_{PCM} refers to the latent heat of a PCM.

The equations pertaining to each segment are solved with the fourth-order Runge–Kutta technique in MATLAB software, as well as the ODE45 solver. This allows for the calculation of the temperatures of brackish water, glass cover, PCM, and absorber plate at each moment. Meanwhile, when calculating the equations, the beginning value for each component is assumed to be the surrounding temperature. The modeling utilizes the parameters and coefficients listed in Table 1.

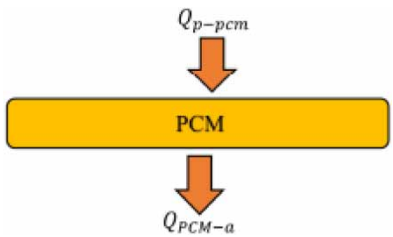

Figure 4 | Schematic diagram of the energy balance related to the PCM.

Table 1 | Solar still parameters

Parameter	Content	Parameter	Content
Type of PCM	Paraffin	$C_{s,PCM}$ (kJ/kg K)	2.87
τ_g	0.88	$C_{l,PCM}$ (kJ/kg K)	2.55
τ_w	0.98	C_w (J/kg K)	4,194
d_0 (°C)	3.15	C_g (J/kg K)	799
T_m (°C)	55.8	C_p (J/kg K)	897
α_g	0.053	x_0 (m)	1
α_w	0.06	k_{ins} (W/m^2 K)	0.038
α_p	0.85	β (°)	32
$L_{s,PCM}$ (kJ/kg)	226.2	A_p (m^2)	1
m_{PCM} (kg)	17.8	k_w (W/m^2 K)	0.6
k_{PCM} (W/m^2 K)	0.26	x_w (m)	0.03
x_{PCM} (m)	0.0212	$C_{s,PCM}$ (kJ/kg K)	2.87
x_{ins} (m)	0.04	Pr_w	9.49
k_p (W/m^2 K)	203.8	U_b (W/m^2 K)	13.8
x_p (m)	0.005	q_w (kg/m^3)	997

2.6. Solar radiation

The solar desalination system derives its energy from solar radiation. The magnitude of this radiation is influenced by various factors, including the geographical coordinates (latitude and longitude), elevation above sea level, and characteristics of the receiving surface. Based on the conducted research, the intensity of solar radiation $I(t)$ for the city of Baghdad on June 28 can be determined by considering the longitude, latitude, and solar time, as mentioned in the reference (Sarhaddi *et al.* 2017).

2.7. Energy equations governing the body system of phase changing matter

In this scenario, the relationships that regulate the system in all components are identical to those in the instance involving a PCM, with the exception of the absorbent plate. The absorbent plate is governed by the connection described in the reference (Sarhaddi *et al.* 2017).

$$Ir_p = Ex_{des,p} = \alpha_p \tau_g \tau_w Ex_{sun} - Ex_{p-w} - Ex_{p-ins} - \frac{dEx_p}{dt} \tag{10}$$

$$Ex_{p-ins} = \left(\frac{k_{PCM}}{x_{PCM}}\right) A_p (T_p - T_{PCM}) \left(1 - \frac{T_a + 273}{T_p + 273}\right) \tag{11}$$

The overall thermal efficiency of the passive desalination system is determined by dividing the amount of heat transferred through evaporation by the total amount of solar energy input. The system can be described in the following manner (Sarhaddi *et al.* 2017):

$$\eta_{th} = \frac{\sum \dot{m}_{ew} hf_g}{3,600 A_p \sum I(t)} \tag{12}$$

The term 'dt' refers to the specific duration of time in which solar radiation is present.

$$\dot{m}_{ew} = \frac{h_{ew} A_w (t_w - t_g) 3,600}{hf_g} \tag{13}$$

By calculating the specified equations, the temperature of various components of the system is determined. Equation (12) can be used to determine the latent heat of evaporation of evaporated water, which is essential for estimating the mass of fresh

water generated, using the acquired temperatures.

$$hf_g = 2.4935x(10^6 - 947.79T_i + 0.13132T_i^2 - 0.0047974T_i^3),\ T_i \le 70$$
$$hf_g = 3.1615(10^6 - 761.6T_i),\ T_i \ge 70 \quad (14)$$

T_i is the average temperature of water and glass, which is obtained from the relation.

$$T_i = \frac{T_g + T_w}{2} \quad (15)$$

2.8. Thermal and electrical analysis of the thermal photovoltaic collector

The objective of doing thermal analysis on the thermal photovoltaic collector is to derive equations that may be used to calculate key parameters, including the surface temperature of the solar module, the outlet temperature, and the rate of heat absorbed by the collector. By formulating the energy balance equations for various elements of the thermal photovoltaic collector, such as the photovoltaic cell layer, the absorbent plate, and the fluid flow inside the channel, one may get mathematical expressions for the temperature of these components. The thermal photovoltaic collector's absorbed usable heat rate is determined using Equation (16):

$$\dot{Q}_c = F_R bL[(\alpha\tau)_{eff} G_c - u_l(T_{f,in} - T_a)]$$
$$F_R = \frac{\dot{m}C_p}{u_l bL}\left[1 - \exp\left(\frac{-F' u_l bL}{\dot{m}C_p}\right)\right] \quad (16)$$

The following parameters are denoted by relation (16): heat extraction coefficient (F_R), collector width (b), collector length (L), absorption coefficient of effective transfer ($(\alpha\tau)_{eff}$), solar radiation intensity on the collector (G_c), total heat loss coefficient of the collector (u_l), inlet water temperature to the collector ($T_{f,in}$), ambient temperature (T_a), and collector efficiency coefficient (F'). The preferred approach for calculating each one is provided in the reference (Zhang *et al.* 2023). The previous research studies have identified certain limitations in the electrical analysis methodology. Under conditions of low solar radiation intensity, the electrical efficiency of the photovoltaic module remains the same as the electrical efficiency under reference conditions. Furthermore, it fails to provide a comprehensive explanation of the alterations in electrical characteristics, such as the open circuit voltage, short circuit current, and the voltage and current at the maximum power point. This study employs the four-parameter voltage current model to determine the efficiency of the photovoltaic module. Equation (17) describes the four-parameter model of the solar cell (I–V) curve.

$$I = I_L - I_O\left[\exp\left(\frac{V + IR_S}{a}\right) - 1\right] \quad (17)$$

The model consists of four parameters: series resistance R_S, optical current I_L, reverse saturation current I_O, and desirability factor α. In order to determine the needed four parameters, Equations (18)–(21) are utilized (Zhang *et al.* 2023).

$$I_{L,ref} = I_{sc,ref}$$
$$I_{O,ref} = \frac{I_{sc,ref}}{\exp(V_{oc,ref}/a_{ref})}$$
$$a_{ref} = \frac{2V_{mp,ref} - V_{oc,ref}}{\left(\frac{I_{mp,ref}}{I_{sc,ref} - I_{mp,ref}}\right) + \mathrm{Ln}\left(1 - \frac{I_{mp,ref}}{I_{sc,ref}}\right)} \quad (18)$$
$$R_{S,ref} = \frac{a_{ref}\mathrm{Ln}\left(1 - \frac{I_{mp,ref}}{I_{sc,ref}}\right) + V_{oc,ref} - V_{mp,ref}}{I_{mp,ref}}$$

In the reference conditions, the values of $I_{mp,ref}$, $V_{mp,ref}$, $I_{sc,ref}$, and $V_{oc,ref}$ are provided by the manufacturers of photovoltaic modules. A series of transfer equations are used to calculate the parameters.

3. ECONOMIC ANALYSIS

Economic study calculates the cost of producing one liter of water. The economic analysis conducted by Fatt *et al.* (Bekheet *et al.* 2023) has been utilized in this research. Several factors influence the cost of producing fresh water in solar desalination systems. These include the return-on-investment coefficient, the coefficient of capital decline, annual fixed cost, salvage value, annual salvage value, annual maintenance and repair costs, and annual cost per square meter. These parameters can be calculated using Equations (19)–(25), respectively.

$$\mathrm{CRF} = \frac{i(1+i)^n}{(1+i)^n - 1} \tag{19}$$

$$\mathrm{SFF} = \frac{i}{(1+i)^n - 1} \tag{20}$$

$$\mathrm{AFC} = \mathrm{CRF}(P) \tag{21}$$

$$S = 0.1(P) \tag{22}$$

$$\mathrm{ASC} = \mathrm{SFF}(S) \tag{23}$$

$$\mathrm{AMC} = 0.15(\mathrm{AFC}) \tag{24}$$

$$\mathrm{TAC} = \mathrm{AFC} - \mathrm{ASC} + \mathrm{AMC} \tag{25}$$

In Equations (19)–(25), the variables n, i, and P represent the lifetime of the device, the discount rate, and the investment cost, respectively. In the economic study conducted by Fatt and his colleagues (Bekheet *et al.* 2023), daily freshwater production is multiplied by 365 to get annual production.

4. RESULTS AND DISCUSSION

4.1. Model validation and performance analysis

This section delves into the validation of the mathematical model and analyzes the performance of the inclined step solar desalination system. The results obtained from the current study are compared with those reported by Sarhaddi *et al.* (2017) to assess the model's accuracy. The RMSE is employed as a quantitative metric to evaluate the agreement between the modeled and reference data. Following the validation process, a systematic analysis of the factors influencing the system's performance is presented. This analysis provides insights into the key parameters that govern the desalination efficiency.

- Temperature profile comparison

Figure 5 presents the temporal variations in salt water temperature for three scenarios: the current study, the study by Sarhaddi *et al.* (2017), and experimental data. This figure serves as a visual comparison of the temperature profiles obtained

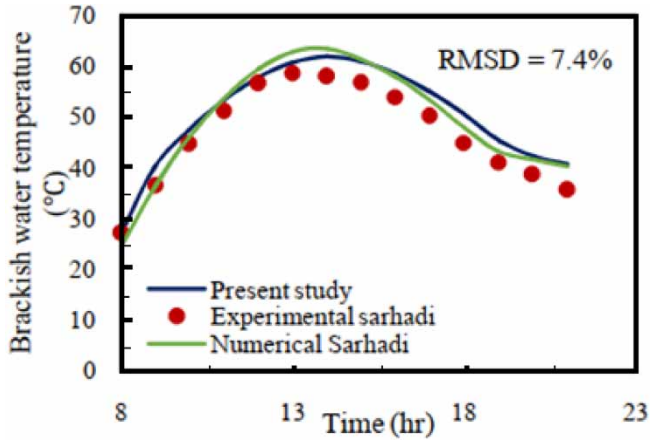

Figure 5 | Changes in salt water temperature with respect to time for the present study, the Sarhadi study, and the experimental data.

from these different sources. It allows for a direct assessment of the modeling approach employed in this work by evaluating its consistency with the reference study and real-world observations. By analyzing the trends and patterns in the salt water temperature profiles, any discrepancies or agreements between the datasets can be identified. Such an evaluation helps to establish the effectiveness of the present modeling methodology and its fidelity in replicating actual system behavior.

Figure 6 depicts the temporal variations in the glass cover temperature for the present study, a reference study (Sarhaddi *et al*. 2017), and experimental data. This comparison allows for an assessment of the modeling approach's ability to predict the thermal behavior of the glass cover. By analyzing the trends in the temperature profiles, discrepancies or agreements between the datasets can be identified. Such an evaluation helps to determine the model's effectiveness in capturing the glass cover's dynamic temperature response.

The close agreement between the simulated values and the experimental data observed in Figures 5 and 6 demonstrates the efficacy of the employed modeling approach. A comprehensive evaluation of the model's performance is achieved by analyzing both figures concurrently. This comparative analysis considers the temperature profiles for both the salt water and the glass cover, allowing for an assessment of the model's accuracy, reliability, and ability to capture the system's thermal behavior. This validation process strengthens the confidence in the methodology used and the results obtained in the present study.

Figure 7 depicts system-produced fresh water accumulation. As it is known, in general, the amount of fresh water produced by the system without PCM is less than when the system is equipped with such substances. Also, in the absence of solar radiation, i.e., 19:00 to 21:00, due to the reverse heat transfer, i.e., from the PCM to the absorbent plate and salt water, the system

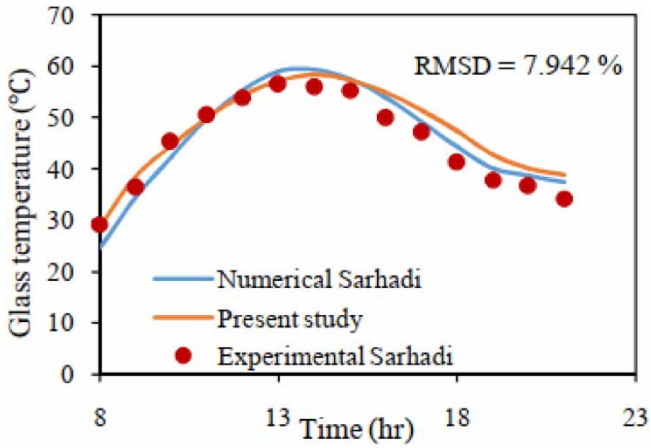

Figure 6 | Changes in the temperature of the glass cover over time for the present study, the border study, and the experimental data.

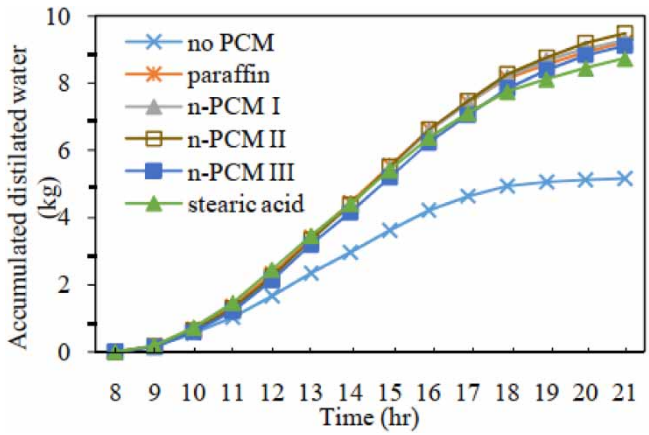

Figure 7 | Daily freshwater production under fixed conditions.

will continue to desalinate the water. When PCM material is present, surface evaporation of water results in more equal heat transfer. The fact that the PCM material absorbs heat during the day and becomes liquid is also the most crucial factor. This heat is retained in it, and when night falls and sunlight is no longer available to produce heat, this substance releases its energy as heat through its transformation from liquid to solid, producing the necessary heat.

In addition, as it can be seen from the figure, the slope of the curve is almost constant in the absence of PCM, but in the presence of such materials, it has an upward trend, which indicates the production of fresh water in the absence of solar radiation. Figure 8 displays the system's hourly rate of freshwater generation under different fixed circumstances, while incorporating various PCMs. It is evident that the system exhibits enhanced performance in the presence of these chemicals. Upon the system's activation, the output rate escalates and attains its peak value between 13:00 and 14:00, coinciding with the zenith of solar radiation.

According to Figure 9, it can be seen that the amount of treated water per day (kg/m^2 h) is displayed for different types of PCM at different salt water flow rates. These materials include PCM-free, paraffin, *n*-PCM I, *n*-PCM II, *n*-PCM III, and stearic acid. As can be seen, *n*-PCM II can play a more effective role in the studied water desalination system, and the most production is dedicated to this PCM. As the brine flow rate increases from 0.07 to 0.4 kg/min, the daily amount of treated water decreases for all PCMs.

Figure 10 demonstrates that the temperature of the PCM gradually rises over time when solar radiation begins, eventually reaching its melting point. The rate at which the PCM reaches its melting point is determined by its thermal conductivity

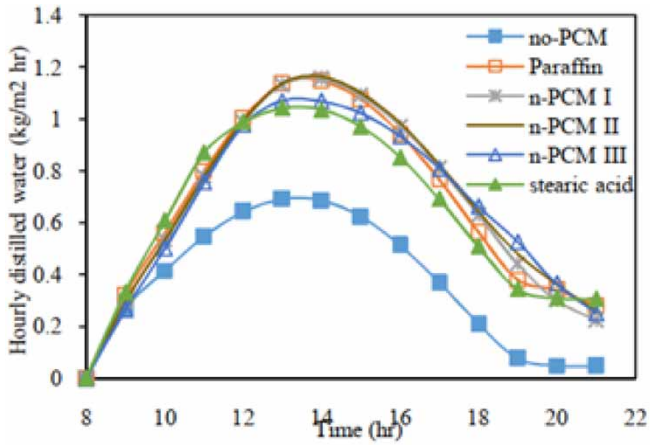

Figure 8 | Hourly rate of freshwater production during system operation for different PCMs.

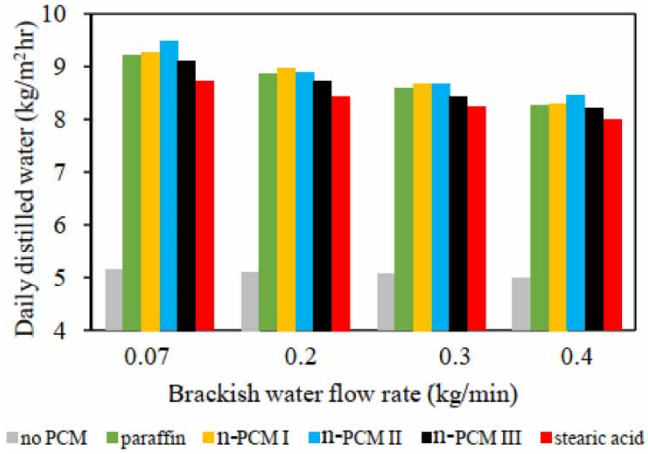

Figure 9 | Daily freshwater production by flow rate and PCM.

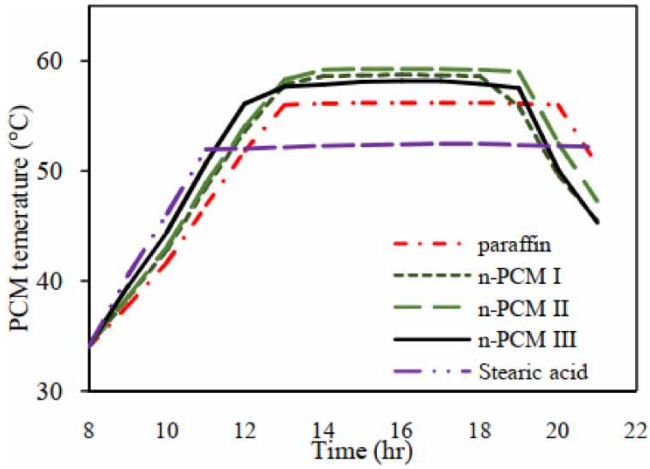

Figure 10 | Changes in the temperature of the PCM with time.

coefficient. A higher coefficient means that the material absorbs heat from the absorbent plate more quickly, leading to a faster temperature increase. Additionally, the material's latent heat capacity plays a role. A larger capacity allows the material to store more heat within itself.

In this case, according to Figure 10, the high latent heat of stearic acid prevents it from transitioning to a solid phase until 21:00, meaning it continues to provide sensible heat to the system during the hours following the temperature change. Figure 11 illustrates the energy efficiency of the system under varying flow rates and with different PCMs. The energy range for *n*-PCM II is 55.63 and 79.56% at flow rates of 0.07 and 0.4, respectively.

The graphs demonstrate that, in comparison to the other PCMs, *n*-PCM II performs the best and produces the most freshwater. This can be explained by the fact that, in comparison to other materials, this PCM has the largest specific heat capacity and thermal conductivity coefficient. A substance with a high specific heat capacity can store the greatest heat in a given mass and use that heat for an extended amount of time. This also makes it possible for thermal energy needed for seawater desalination to be available for longer during the night.

The situation with the maximum efficiency occurs when the *n*-PCM I phase change nanomaterial is utilized, at flow rates of 0.2 and 0.3 kg/min. The energy efficiency values are 28.60 and 31.58%, respectively. It is important to mention that the aforementioned results are provided for constant values of ambient temperature, wind speed, and thickness of the PCM depicted in the image.

As previously indicated, *n*-PCM II is the best material, followed by *n*-PCM I and *n*-PCM III. This discrepancy can be attributed mostly to the fact that *n*-PCM II material has a greater thermal conductivity coefficient than *n*-PCM I, and *n*-PCM I has a

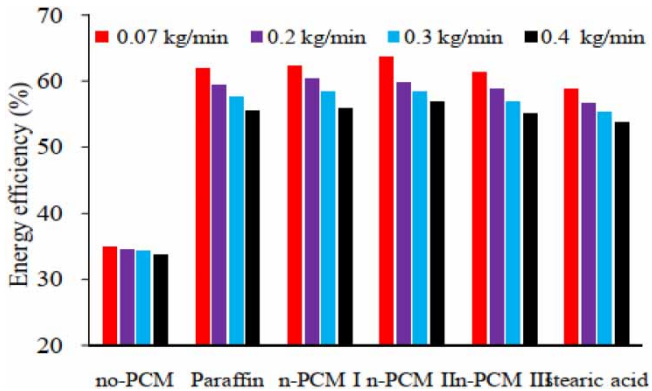

Figure 11 | Energy efficiency of the system at different flow rates and for different PCMs.

higher thermal conductivity coefficient than *n*-PCM III. Consequently, *n*-PCM II has the largest water output. Because *n*-PCM III material has a larger specific heat capacity than other materials, it has also been noted that using this material creates more stable water than using other materials.

4.2. Analysis of economic results

To assess water production under extreme conditions, we investigated freshwater production on a hot summer day in July and a cold winter day. The production rates were 5.6 and 1.2 kg/h, respectively. These values were used as a basis for estimating the cost of water production during peak demand periods throughout the year for economic calculations. Table 2 displays the

Table 2 | Estimated price of the system under review

Components	Amount	Unit price ($)	Total price ($)
4 mm thick glass	3 m^2	1.9	5.7
Thermal photovoltaic collector	1	190.5	190.5
PCM	40 kg	0.71	2.9
Galvanized steel sheet	4 m^2	3	12
Water pump	1	47.6	47.6
Galvanized pipe	4 m	2.9	11.42
Manpower	–	–	36
Aquarium glue	2	2.4	4.8
Insulation	4 m^2	0.48	1.5
Total price	–	–	337

Table 3 | Economic analysis of the present study and comparison with other studies

Economic parameters	Unit	Faegh *et al.* (Faegh & Shafii 2017)	Mosleh *et al.* (2015)	Current study
Investment cost (p)	$	206	568	337
Salvage value (10% of initial capital) (S)	$	206	56.8	33.7
Device lifetime (n)	years	20	20	20
Discount rate (i)	(%)	10	10	10
Return on investment	–	0.117	0.117	0.177
Capital decline coefficient	–	0.0175	0.0175	0.0175
Fixed annual fee	$	24.10	66.72	39.42
Annual cancellation fee	–	0.350	0.992	0.589
Annual maintenance and repair cost (15% of the annual fixed cost)	$	3.61	10.01	5.91
Annual cost per square meter (annual fixed cost + maintenance cost – annual scrapping cost)	$	27.36	75.73	44.74
Daily production of fresh water	l/m^2	3.52	4.03	3.9
Annual production (daily production × 365)	l/m^2	1,288.15	1,585.7	1,423.5
Annual useful energy per surface unit (annual production × latent heat of water vapor) (latent heat of water vapor – kWh/L 0.65)	kW·h/m^2	837.3	1,030.7	925.2
Distilled water cost as per liter in square meter of heat absorption plate (year fixed cost on yearly production)	$	0.0187	0.0421	0.0276
Distilled water cost for kilowatt hour in square meter of heat absorption plate (year fixed cost on yearly operable energy level)	$	0.0287	0.0647	0.426
Price for every liter as fresh water	$/l	0.0212	0.0478	0.0314

comprehensive cost of the device, encompassing the expenses for equipment, welding, and labor. It also presents the individual prices of each component and the expected overall price. To facilitate an economic comparison between the current research and other projects, the total cost of the gadget is estimated to be approximately $337, based on the prevailing daily exchange rate of the Iraqi currency.

Table 3 presents the economic calculations pertaining to the current study, as well as the research conducted by Faiq *et al.* (Amani & Kolliopoulos 2023) and Jafari Mosleh *et al.* (Aghajani Afghan *et al*. 2023). Economics studies showed that the value per surface unit for this study is 0.0314 $/l of fresh water. Additionally, the cost of freshwater production, based on the research by Faegh *et al.* (Amani & Kolliopoulos 2023) and Jafari Mosleh and colleagues (Aghajani Afghan *et al*. 2023), is 0.0212 and 0.0478 $/L, respectively.

Based on the current exchange rate of the dollar in Iraq, the price of fresh water generated for the present study is within a reasonable range. It can be argued that the cost of a mineral water is indicative of the economic viability of the associated water desalination device.

5. CONCLUSION

Overall, using PCM enhances the efficiency of the solar desalination system, resulting in higher output rates. In the absence of a phase changer, the rate of freshwater production is around 5.15 kg/m^2 h. However, when various phase changers such as paraffin *n*-PCM I, *n*-PCM II, *n*-PCM III, and stearic acid are present, the rates increase to 22.9, 28.9, and 5.9 kg/m^2 h, respectively. The values are 11.9 and 78.3 kg/m^2 h. The energy efficiency of *n*-PCM II, a composite of paraffin and copper oxide nanoparticles, is approximately 55.63 and 79.56% for input flow rates of 0.07 and 0.4, respectively. It outperforms other PCMs in terms of energy efficiency. When the input flow rates are 0.2 and 0.3 kg/min, the *n*-PCM I, which consists of paraffin and copper oxide, achieves energy efficiencies of 28.60 and 31.58%, respectively. These efficiencies surpass those of other materials, indicating superior performance. The economic analysis done and comparison with similar research shows that the studied system is economically viable.

CONSENT FOR PUBLICATION

The authors give their full consent for the publication of this manuscript.

ACKNOWLEDGEMENTS

The authors extend their appreciation to Cihan University-Erbil, Iraq and to the Researchers Supporting Project number (RSPD2024R620), King Saud University, Riyadh, Saudi Arabia.

DATA AVAILABILITY STATEMENT

All relevant data are included in the paper or its Supplementary Information.

CONFLICT OF INTEREST

The authors declare there is no conflict.

REFERENCES

Aghajani Afghan, S., Shafaghat, R., Aghajani Afghan, A. & Hosseinalipour, S. M. 2023 An experimental study to apply an absorption refrigeration cycle as a dehumidifier in humidification-dehumidification solar desalination system. *Iranian (Iranica) Journal of Energy & Environment* **14** (4), 361–371.

Alhamami, A. H., Falude, E., Ibrahim, A. O., Dodo, Y. A., Daniel, O. L. & Atamurotov, F. 2024 Solar desalination system for fresh water production performance estimation in net-zero energy consumption building: A comparative study on various machine learning models. *Water Science & Technology* **89** (8), 2149–2163.

Al-harahsheh, M., Abu-Arabi, M., Mousa, H. & Alzghoul, Z. 2018 Solar desalination using solar still enhanced by external solar collector and PCM. *Applied Thermal Engineering* **128**, 1030–1040.

Al-Kharabsheh, S. & Yogi, D. 2003 Analysis of an innovative water desalination system using low-grade solar heat. *Desalination* **156** (1–3), 323–332.

Amani, A. & Kolliopoulos, G. 2023 Modeling of transport phenomena in a hybrid forward osmosis-directional freeze crystallization process for clean water recovery from hydrometallurgical effluents. *Water Science & Technology* **88** (7), 1657–1671.

Asbik, M., Ansari, O., Bah, A., Zari, N., Mimet, A. & El-Ghetany, H. 2016 Exergy analysis of solar desalination still combined with heat storage system using phase change material (PCM). *Desalination* **381**, 26–37.

Bekheet, H. N., Al Sudany, N. K. & Najm, S. S. 2023 Iraqi economy and renewable energy projects between economic necessity and investment challenges. *International Journal of Professional Business Review* **8** (8), 71.

Boukhriss, M., Maatoug, M. A., Farhani, S., Timoumi, M., Jammali, A. & Bacha, H. B. 2023 Experimental validation of membrane distillation unit coupled with a sweeping gas membrane using solar energy. *International Journal of Low-Carbon Technologies* **18**, 999–1007.

Bressmann, T. 2004 Self-inflicted cosmetic tongue split: A case report. *Journal of the Canadian Dental Association* **70** (3), 156–157.

Dhivagar, R., Mohanraj, M., Raj, P. & Gopidesi, R. K. 2021 Thermodynamic analysis of single slope solar still using graphite plates and block magnets at seasonal climatic conditions. *Water Science and Technology* **84** (10–11), 2635–2651.

El-Samadony, Y., Abdullah, A. & Omara, Z. 2015 Experimental study of stepped solar still integrated with reflectors and external condenser. *Experimental Heat Transfer* **28** (4), 392–404.

Faegh, M. & Shafii, M. B. 2017 Experimental investigation of a solar still equipped with an external heat storage system using phase change materials and heat pipes. *Desalination* **409**, 128–135.

Fath, H. E. & Hosny, H. 2002 Thermal performance of a single-sloped basin still with an inherent built-in additional condenser. *Desalination* **142** (1), 19–27.

Fayaz, H., Ramesh, S., Afzal, A., Ağbulut, Ü., Khan, S. A., Asif, M., Raja, V. & Linul, E. 2024 Investigation of numerical phase transition of nano-enhanced SiC/paraffin wax PCM in solar-assisted water desalination system. *Thermal Science and Engineering Progress* **50**, 102528.

Hansen, R. S. & Murugavel, K. K. 2017 Enhancement of integrated solar still using different new absorber configurations: An experimental approach. *Desalination* **422**, 59–67.

Ibrahim, A. G., Rashad, A. M. & Dincer, I. 2017 Exergoeconomic analysis for cost optimization of a solar distillation system. *Solar Energy* **151**, 22–32.

Kabeel, A. 2009 Performance of solar still with a concave wick evaporation surface. *Energy* **34** (10), 1504–1509.

Kabeel, A. & Abdelgaied, M. 2016 Improving the performance of solar still by using PCM as a thermal storage medium under Egyptian conditions. *Desalination* **383**, 22–28.

Kabeel, A., El-Agouz, S. A., Sathyamurthy, R. & Arunkumar, T. 2018 Augmenting the productivity of solar still using jute cloth knitted with sand heat energy storage. *Desalination* **443**, 122–129.

Kalogirou, S. A. 2005 Seawater desalination using renewable energy sources. *Progress in Energy and Combustion Science* **31** (3), 242–281.

Khalifa, A. J. N. & Ibrahim, H. A. 2009 Effect of inclination of the external reflector on the performance of a basin type solar still at various seasons. *Energy for Sustainable Development* **13** (4), 244–249.

Loreti Hupsel, A., Borges, C. P., da Fonseca, F. V. & Barbosa, G. M. 2024 Evaluation of pretreatment routes for seawater desalination by nanofiltration. *Water Science & Technology* **89** (2), 454–469.

Majumder, S., Sadashiva Murthy, B. M. & Prakash, B. M. 2023 Impact of different electrodes, mediators, and microbial cultures on wastewater treatment and power generation in the microbial desalination cell (MDC). *Water Science & Technology* **88** (12), 3194–3225.

Mishra, R. K. 2023 Fresh water availability and its global challenge. *British Journal of Multidisciplinary and Advanced Studies* **4** (3), 1–78.

Mishra, B. K., Kumar, P., Saraswat, C., Chakraborty, S. & Gautam, A. 2021 Water security in a changing environment: Concept, challenges and solutions. *Water* **13** (4), 490.

Mosleh, H. J., Mamouri, S. J., Shafii, M. B. & Sima, A. H. 2015 A new desalination system using a combination of heat pipe, evacuated tube and parabolic trough collector. *Energy Conversion and Management* **99**, 141–150.

Rabhi, K., Nciri, R., Nasri, F., Ali, C. & Bacha, H. B. 2017 Experimental performance analysis of a modified single-basin single-slope solar still with pin fins absorber and condenser. *Desalination* **416**, 86–93.

Rahbar, N., Gharaiian, A. & Rashidi, S. 2017 Exergy and economic analysis for a double slope solar still equipped by thermoelectric heating modules – An experimental investigation. *Desalination* **420**, 106–113.

Rezaei Rad, M., Shafaghat, R., Aghajani Afghan, A. & Alizadeh Kharkeshi, B. 2023 An experimental study to evaluate the performance of an HDH water desalination system with a thermoelectric condenser. *Renewable Energy Research and Applications*. https://doi.org/10.22044/rera.2023.12548.1191.

Saadi, Z., Rahmani, A., Lachtar, S. & Soualmi, H. 2018 Performance evaluation of a new stepped solar still under the desert climatic conditions. *Energy Conversion and Management* **171**, 1749–1760.

Sarhaddi, F., Tabrizi, F. F., Zoori, H. A. & Mousavi, S. A. H. S. 2017 Comparative study of two weir type cascade solar stills with and without PCM storage using energy and exergy analysis. *Energy Conversion and Management* **133**, 97–109.

Shanmugan, S., Hammoodi, K. A., Eswarlal, T., Selvaraju, P., Bendoukha, S., Barhoumi, N., Mansour, M., Refaey, H. A., Rao, M. C., Mourad, A. I., Fuji, M. & Elsheikh, A. 2024 A technical appraisal of solar photovoltaic-integrated single slope single basin solar still for simultaneous energy and water generation. *Case Studies in Thermal Engineering* **54**, 104032.

Sharon, H., Reddy, K. S., Krithika, D. & Philip, L. 2017 Experimental performance investigation of tilted solar still with basin and wick for distillate quality and enviro-economic aspects. *Desalination* **410**, 30–54.

Srinivas, P., Aramani, R. A., Allam Ramakrishna, D., Kasthuri, D. K., Swamy, G. K. & Lakshmipathi, A. 2016 Significance of Jala Mahabhuta (Water) in day to day life. *WJPPS* **5** (3), 1781–1793.

Tamini, A. 1987 Performance of a solar still with reflectors and black dye. *Solar & Wind Technology* **4** (4), 443–446.

Tanaka, H. 2009a Experimental study of a basin type solar still with internal and external reflectors in winter. *Desalination* **249** (1), 130–134.
Tanaka, H. 2009b Effect of inclination of external reflector of basin type still in summer. *Desalination* **242** (1–3), 205–214.
Tiwari, G. & Sahota, L. 2017 *Advanced Solar-Distillation Systems: Basic Principles, Thermal Modeling, and Its Application*. Springer, Singapore. https://doi.org/10.1007/978-981-10-4672-8.
Tiwari, G., Kupfermann, A. & Aggarwal, S. 1997 A new design for a double-condensing chamber solar still. *Desalination* **114** (2), 153–164.
Tsani, S., Koundouri, P. & Akinsete, E. 2020 Resource management and sustainable development: A review of the European water policies in accordance with the United Nations' Sustainable Development Goals. *Environmental Science & Policy* **114**, 570–579.
Yang, Y., Ren, X., Li, Y., Yuan, D., Guo, Y., Zhang, K. & Shen, S. 2023 Thermal optimization research of vertical tube climbing film desalination system. *International Journal of Low-Carbon Technologies* **18**, 473–481.
Yazdanpanahi, J. & Sarhaddi, F. 2017 Irreversibility rates in a solar photovoltaic/thermal water collector: An experimental study. *Heat Transfer Research* **48** (8), 741–756.
Zamani, M., Shafaghat, R. & Kharkeshi, B. A. 2023a Experimental investigation on the effect of flow rate and load on the hydrodynamic behavior and performance of an archimedes screw turbine. *International Journal of Engineering* **36** (4), 733–745.
Zamani, M., Shafaghat, R. & Alizadeh Kharkeshi, B. 2023b Numerical study of the hydrodynamic behavior of an archimedes screw turbine by experimental data in order to optimize turbine performance: The genetic algorithm. *Journal of Applied and Computational Mechanics* **9** (4), 1060–1075.
Zhang, X., Li, H. & Taghavi, M. 2023 Exergoeconomic evaluation of a new carbon-free hydrogen and freshwater production system based on biomass gasification process. *International Journal of Low-Carbon Technologies* **18**, 589–599.

First received 18 February 2024; accepted in revised form 10 May 2024. Available online 24 May 2024